Absorption, Excitation and Emission Spectra of SrCl2:Eu2+

ARTICLE *in* CHEMICAL PHYSICS LETTERS · SEPTEMBER 2006

Impact Factor: 1.9 · DOI: 10.1016/j.cplett.2006.07.029

Available online at www.sciencedirect.com
ScienceDirect
Chemical Physics Letters 428 (2006) 78–82
CHEMICAL PHYSICS LETTERS
www.elsevier.com/locate/cplett

Absorption, excitation and emission spectra of $SrCl_2:Eu^{2+}$

Zaifa Pan [a], Lixin Ning [a], Bing-Ming Cheng [b], Peter A. Tanner [a,*]

[a] Department of Biology and Chemistry, City University of Hong Kong, Tat Chee Avenue, Kowloon, Hong Kong S.A.R., China
[b] National Synchrotron Radiation Research Center, 101 Hsin-Ann Road, Hsinchu Science Park, Hsinchu 30076, Taiwan, ROC

Received 29 May 2006; in final form 10 July 2006
Available online 15 July 2006

Abstract

The 10 K ultraviolet emission spectrum and low-energy ultraviolet absorption spectra are reported for dilute $SrCl_2:Eu^{2+}$. Only one luminescent state is observed under various synchrotron radiation excitation wavelengths. The broad room temperature $4f^65d \rightarrow 4f^7$ emission spectrum, peaking at 410 nm, sharpens considerably at 10 K and vibrational progressions in the totally symmetric Sr–Cl stretching mode of 210 cm^{-1} upon the zero phonon line and vibronic structure are predominant. The low-energy $4f^7 \rightarrow 4f^65d$ absorption spectrum comprises similar vibronic structure but many transitions overlap. The emission, absorption and excitation spectra are well simulated by calculation.

1. Introduction

The clearly-written review of Rubio O [1] documented the studies of the electronic spectra of Eu^{2+} doped into alkali and alkaline earth halides. Generally for the chloride systems, an intense emission band was observed at ~400 nm which corresponds to the electric dipole allowed transition $4f^65d \rightarrow 4f^7$. There is only one short report of a study at liquid helium temperature [2], that of $SrCl_2:Eu^{2+}$, and the peaks in the emission band were labeled with separations between 96 and 111 cm^{-1}. This was surprising to us because the d–f emission spectra of Tm^{2+} [3] and Sm^{2+} [4] diluted into $SrCl_2$ show vibrational progressions in a mode of ~210 cm^{-1}. We therefore decided to reinvestigate the electronic spectra of Eu^{2+} both experimentally and theoretically. Following the review of Rubio O, subsequent publications on $SrCl_2:Eu^{2+}$ have concerned the emission lifetime and quantum efficiency of $d \rightarrow f$ emission [5] and the photostimulated luminescence of $SrCl_2:Eu^{2+}$ doped with Na^+ ions [6]. Recently, there is a burgeoning interest in the luminescence of Eu^{2+} and its applications for persistent luminescence [7] and white light-emitting-diode illumination [8].

2. Experimental

The samples of $SrCl_2:Eu^{2+}$(nominal 0.05 at.%) were prepared by the solid-state reaction of the starting materials of $SrCl_2$, Eu_2O_3 and activated charcoal in stoichiometric quantities. Eu_2O_3 (1.66 mg; Strem Chemicals, 99.99%) was dissolved in a beaker with (250 cm^3) hot concentrated hydrochloric acid (37%, Riedel-de Haën, RG). Then $SrCl_2$ (3.0000 g; Aldrich Chemicals, 99.995%) was added and the mixture was evaporated to dryness. The solid obtained was ground into a powder by a glass rod under strong heating in order to exclude moisture. Activated charcoal (0.03 mg; Panreac Quimica, SA) was then mixed with the salts. The powder was transferred to a preheated clean quartz tube and heated under vacuum at 673 K. The tube was sealed off as an ampoule and lowered through the Bridgman furnace at 1170 K at a rate 1.2 cm h^{-1}. Subsequently, the tube was opened in a nitrogen atmosphere. A clear part of the crystal was polished and coated with Pattex transparent contact adhesive for protection.

Room temperature emission spectra (resolution ~3 nm) was recorded by a Jobin–Yvon Fluoromax-3 spectrofluo-

* Corresponding author. Fax: +852 2788 7406.
E-mail address: bhtan@cityu.edu.hk (P.A. Tanner).

0009-2614/$ - see front matter © 2006 Elsevier B.V. All rights reserved.
doi:10.1016/j.cplett.2006.07.029

rometer and also using the photoluminescence end station coupled to the high flux BL03A synchrotron radiation beam line at the National Synchrotron Radiation Center, Hsinchu, Taiwan [9]. Emission spectra were also recorded from 300 to 10 K at a resolution of 2–4 cm^{-1} using the third harmonic of a Surelite Nd–YAG laser. The crystals were mounted in an Oxford Instruments closed cycle cryostat. The emission was collected at 90° and passed through an Acton 0.5 m spectrometer equipped with a Spectrum charge-coupled device. The single-beam absorption spectra (300–10 K) of a sample were also recorded using Xe and D_2 lamps using the same detection system.

3. Results and discussion

3.1. Description of spectra

The Eu^{2+} ion has the same charge and similar ionic radius (117 pm) as Sr^{2+} (118 pm) so that it substitutes the eight-coordinate cubic symmetry site in $SrCl_2$ without distortion. The electronic ground state of Eu^{2+} in this lattice is $(4f^7)^8S_{7/2}$ and the zero-field splitting is not resolved in our measurements. The room temperature emission spectra of $SrCl_2$:Eu^{2+} excited by synchrotron radiation, and by a xenon lamp, Fig. 1a show a broad feature which has a maximum at 410 nm. The spectrum is similar for excitation by other synchrotron radiation wavelengths. On cooling to 10 K, features are more clearly resolved and their vibrational energy displacements from the zero phonon line are marked in Fig. 1b. Three vibrational energies: 82 ± 2, 118 ± 1 and 210 cm^{-1} are clearly deduced from the spectrum. The 210 cm^{-1} mode forms the most prominent vibrational progressions on the origin and the other vibronic structure. The corresponding progression frequencies in the d–f emission spectra of Tm^{2+} [3], Sm^{2+} [4] and Yb^{2+} [10] doped in $SrCl_2$ are 210, 213 and 213 cm^{-1}, respectively, and are thus almost insensitive to the mass of the lanthanide ion, which is 12% lower for Eu than Yb. The corresponding progression frequency in SrF_2:Sm^{2+} is 292 cm^{-1} [4] which is identical with that calculated from $SrCl_2$:Sm^{2+} using the G-matrix element of either the e_g or a_{1g} vibrational modes of the XY_8 system. Axe [4] assigned this vibration to the e_g mode on the basis that 'not all of the absorption bands of $SrCl_2$:Eu^{2+} show the 213 cm^{-1} interval'. However this assignment of the major vibrational progressions in Ln^{2+} d–f spectra to e_g rather than a_{1g} progressions is not consistent with the d–f spectra of Ln^{3+} [11]. Furthermore, the lattice dynamics calculations of Kühner et al. [12] for the $SrCl_2$:Sm^{2+} system show that the projected density of states of the a_{1g} vibration of the nearest chloride ion neighbours has a sharp peak at 210 cm^{-1}. The bands at 82 ± 2, 118 ± 1 cm^{-1} below the zero phonon line are sharper in a more dilute Eu^{2+} sample and very weak fine structure is also tentatively resolved at 133 and 189 cm^{-1}. The 82, 118 cm^{-1} modes are either associated with the $k = 0$ t_{2g} modes at the zone boundary or with second shell motions.

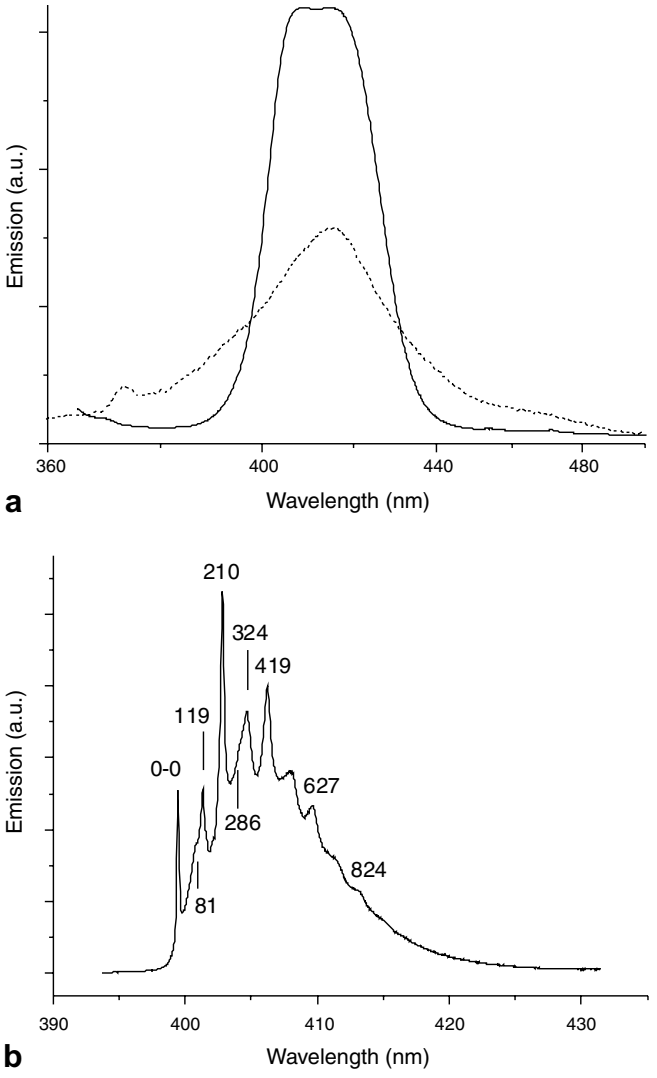

Fig. 1. Emission spectra of $SrCl_2$:Eu^{2+}: (a) room temperature: Xe 355-nm excitation, (full line) and synchrotron radiation 338 nm excitation (dotted line); (b) 10 K Nd–YAG 355 nm excitation. The major vibrational energy displacements from the zero phonon line (0–0) are marked in cm^{-1}.

Fig. 2a shows the first bands in the 10 K single beam absorption spectrum of $SrCl_2$:Eu^{2+}. The zero phonon lines in absorption and emission are coincident. The vibronic structure matches that in emission with similar displacement energies but many transitions overlap. Some electronic states of the $4f^65d$ configuration are identified from the absorption spectrum and are listed in Table 2 in column E_{obs}. The energies are in agreement with the previous tabulation of Freed and Katcoff [13]. A further discussion is given in Section 3.3.

3.2. Calculation of $4f^65d$ energy levels

The calculation of $4f^65d$ energy levels employed the extended f-shell programs of Prof. M.F. Reid, in which various parameterized Hamiltonians for the $4f^65d$ configuration were diagonalized simultaneously to calculate the electronic energy levels. The standard Hamiltonian consists

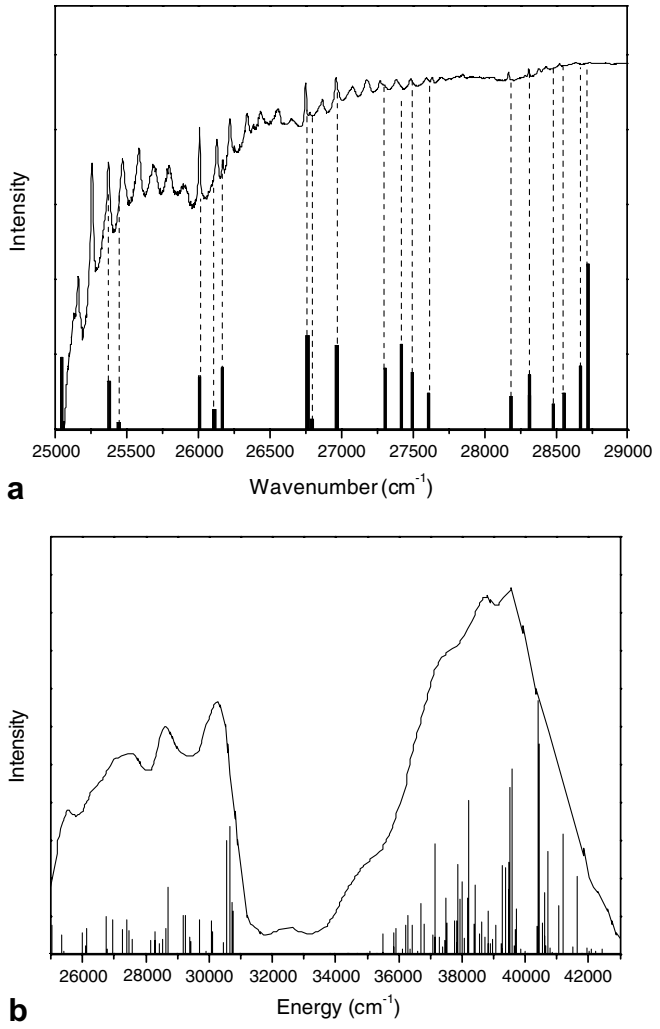

Fig. 2. Experimental and calculated absorption and excitation spectra for the $4f^7 \rightarrow 4f^6 5d$ transitions of Eu^{2+} in $SrCl_2$. The solid curves in (a) and (b) are the experimental absorption spectrum at 10 K of the present work and excitation spectrum at 80 K reproduced from [18], respectively. The solid vertical lines are predicted positions for zero phonon lines with heights proportional to calculated relative oscillator strengths. The correspondence of zero phonon line positions between calculation and experiment is made by the dashed vertical lines in (a).

Table 1
Energy parameters for $4f^6 5d$ configurations of Eu^{2+} in $SrCl_2$

Parameter	cm^{-1}
F^2(ff)	71 803
F^4(ff)[a]	50 514
F^6(ff)[a]	38 896
ζ(f)	1272
α(ff)	[18.6]
β(ff)	[−590]
γ(ff)	[1805]
T^2(ff)	[330]
T^3(ff)	[41.5]
T^4(ff)	[62]
T^6(ff)	[−295]
T^7(ff)	[360]
T^8(ff)	[310]
M^0(ff)	[2.66]
M^2(ff)	[1.54]
M^4(ff)	[1.01]
P^2(ff)	[619]
P^4(ff)	[450]
P^6(ff)	[300]
ζ(d)	844
F^2(fd)	12 330
F^4(fd)	5916
G^1(fd)	5672
G^3(fd)	4539
G^5(fd)	3444
B_0^4(ff)[b]	−1035
B_0^6(ff)[b]	−761
B_0^4(dd)[b]	−21 296

The values in brackets were not allowed to vary in the parameter optimization, and taken from those of Eu^{2+} in SrF_2 [15]. Parameters for f–d interactions were calculated using Cowan's code [16] (but reduced by ~51%). See [14] for parameter definitions.

[a] The ratios, $F^4(ff)/F^2(ff) = 0.704$ and $F^6(ff)/F^2(ff) = 0.542$, are from [15].

[b] The crystal–field Hamiltonians for the 4f and 5d electrons are defined as: $H_{CF}(ff) = B_0^4(ff)\left[C_0^4 + \frac{\sqrt{5}}{\sqrt{14}}(C_4^4 + C_{-4}^4)\right] + B_0^6(ff)\left[C_0^6 - \frac{\sqrt{7}}{\sqrt{2}}(C_4^6 + C_{-4}^6)\right]$ and $H_{CF}(dd) = B_0^4(dd)\left[C_0^4 + \frac{\sqrt{5}}{\sqrt{14}}(C_4^4 + C_{-4}^4)\right]$.

of a radial part which is parametrized and an angular part which is calculated exactly in the programs by group-theoretical and tensor operator techniques. Refer, for example, to the footnote of Table 1 for the parametrized Hamiltonians of the crystal–field interactions of the $4f^6$ core and the 5d electron, respectively. The details of the energy level calculation can be found in [14] and are not repeated here. Interaction parameters of the $4f^6$ core include those for the Coulomb interaction between the 4f electrons, F^k(ff), with the fixed ratios $F^4(ff)/F^2(ff)$ and $F^6(ff)/F^2(ff)$; the spin–orbit interaction, ζ(f); and the crystal–field interaction, B_0^4(ff) and B_0^6(ff). These were determined from optimization with respect to the experimental $4f^6 5d$ energy levels. The values for the F^k(ff) ratios and other parameters of small free–ion interactions of $4f^6$ core were taken from those of the $4f^7$ configuration of Eu^{2+} in SrF_2 [15]. The values of parameters, ζ(d) and B_0^4(dd), for the spin–orbit interaction and crystal–field interaction of the 5d electron, respectively, were also optimized in the calculation. The f–d Coulomb interaction parameters, F^k(fd) and G^k(fd), were calculated from the standard atomic computer programs [16] and then reduced with the overall reduction factor as an optimized parameter. A total of seven parameters were varied simultaneously within certain allowed ranges, and optimized by repeatedly calculating $4f^6 5d$ levels until the best agreement was obtained between the calculated and observed crystal–field level energies. Only the crystal–field levels which were certainly identified from the absorption spectrum (i.e., those shown in normal type in Table 2 in column E_{obs}) were employed in the calculation. The resulting optimized parameters are listed in Table 1, and the calculated and experimental crystal–field levels within the range of 4000 cm^{-1} above the lowest $(4f^6 5d)\Gamma_8$ level are collected in Table 2.

A brief comment on the optimized parameters is made here. The calculated F^k(ff) and ζ(f) values are similar to those of $4f^7$ configuration of Eu^{2+} in SrF_2. This may be

Table 2
Calculated and experimental electronic energy levels for $4f^6 5d$ configuration of Eu^{2+} in $SrCl_2$

$4f^6 5d$ level	Energy above 25044 cm^{-1}			Calculated relative oscillator strength from $(4f^7)^8S_{7/2}$ levels
	E_{calc}	E_{obs} (I)[a]	E_{obs}[b]	
Γ_8	0	−11 (0.8)	0	1.0
Γ_7	327	*329 (0.9)*	*327*	0.67
Γ_8	396	–	–	0.1
Γ_7	960	967 (1.0)	962	0.74
Γ_6	1062	–	–	0.29
Γ_8	1120	1133 (0.3)	1129	0.87
Γ_8	1714	1705 (1.0)	1705	1.31
Γ_6	1745	–	1735	0.15
Γ_8	1918	*1916 (1.0)*	*1918*	1.17
Γ_8	2260	*2225 (0.7)*	*2247*	0.86
Γ_7	2370	*2342 (0.7)*	*2363*	1.18
Γ_8	2446	*2437 (0.7)*	*2437*	0.80
Γ_6	2560	2595 (0.7)	2589	0.51
Γ_8	3139	3125 (0.9)	3121	0.47
Γ_6	3264	–	–	0.48
Γ_7	3265	3267 (0.9)	3265	0.77
Γ_6	3432	*3382 (0.7)*	*3383*	0.36
Γ_8	3506	–	–	0.51
Γ_7	3624	–	–	0.89
Γ_8	3674			2.30

Only the levels within the range of 4000 cm^{-1} above the lowest ($4f^6 5d$) Γ_8 level at 25044 cm^{-1} are included. The levels in italics were not included in the fitting procedure.

[a] E_{obs} (I) Observed energy and intensity from the photographic measurements at 20 K in [13].

[b] E_{obs} Observed energy from this study.

linked to the fact that a more contracted 4f orbital in the $4f^6$ core (relative to the configuration) results in larger F^k and ζ(f) values, but nevertheless the reverse effect is introduced by the more covalent chloride as compared to fluoride ligands. The values obtained for the f–d Coulomb interaction parameters are ~49% of the free–ion values. This reduction is similar to that found by Weakliem [17] for the Eu^{2+} ion, which is mainly due to the interaction of the 5d orbital with the crystal bonding electrons. The optimized value for B_0^4(dd), i.e., the crystal–field parameter of the 5d electron, is also similar to the value, −21332 cm^{-1}, calculated from the observed crystal–field splitting of the 5d electron of Eu^{2+} in $SrCl_2$ [18].

3.3. Calculation of $4f^7 \rightarrow 4f^6 5d$ absorption strengths

The transitions from $4f^7$ to $4f^6 5d$ are electric dipole allowed and the formulae for the calculation of the electric dipole transition moments can be found in [19]. In the calculation, the approximation was made that the unpolarized oscillator strength f_{if} for the zero phonon line between the initial $(4f^7)\Gamma_i$ and the final $(4f^6 5d)\Gamma_f$ levels is proportional to the total electric dipole transition line strength, multiplied by the zero phonon line transition wave number, and can be expressed as

$$f_{if} \propto \bar{\nu}_{if} \sum_{q,\gamma_i,\gamma_f} |\langle f^7 \Gamma_i \gamma_i | D_q^1 | f^6 d \Gamma_f \gamma_f \rangle|^2, \quad (1)$$

where the summation is over the polarization q ($q = 0, \pm 1$) and the components γ of the initial and final levels. The zero-field splitting of the $(4f^7)^8S_{7/2}$ level has been neglected, since it is only on the order of a few tenths of a cm^{-1}. From the point group selection rule, all the transitions from the initial $(4f^7)^8S_{7/2}(\Gamma_6 + \Gamma_7 + \Gamma_8)$ state to the final ($4f^6 5d$) Γ_f levels are electric dipole allowed.

The derived relative oscillator strengths for the zero phonon lines in the spectral range of 25000–29000 cm^{-1} are listed in Table 2. The energy levels in normal type in this table were used in the optimization procedure. The energy levels in italics were also deduced from the spectral analysis but were not fitted, so as to provide a test of the accuracy of the calculation. As shown in Fig. 2a, the calculated transition energies and relative oscillator strengths of zero phonon lines are represented by the solid vertical lines, with heights proportional to calculated relative oscillator strengths. A correspondence of transition energies of zero phonon lines between calculation and experiment is indicated by the dashed vertical lines. The agreement is satisfactory in view of the congestion of energy levels.

In Fig. 2b, the calculated energy positions and relative oscillator strengths in the spectral range of 25000–43000 cm^{-1} are presented. The vibrational progressions are omitted for clarity. Also shown in this figure is the experimental excitation spectrum at 80 K, which was reproduced from [18]. The calculation succeeds in reproducing the gap between the two main excitation bands.

3.4. Simulation of the $4f^6 5d \rightarrow 4f^7$ emission spectrum

The solid curve in Fig. 3 represents the experimental emission spectrum from the lowest $(4f^6 5d)\Gamma_8$ level to the $(4f^7)^8S_{7/2}$ level. For simplicity, we interpret the main features of this spectrum by the electronic $(4f^6 5d)\Gamma_8 \rightarrow (4f^7)^8S_{7/2}$ transition coupled to two local vibrational modes

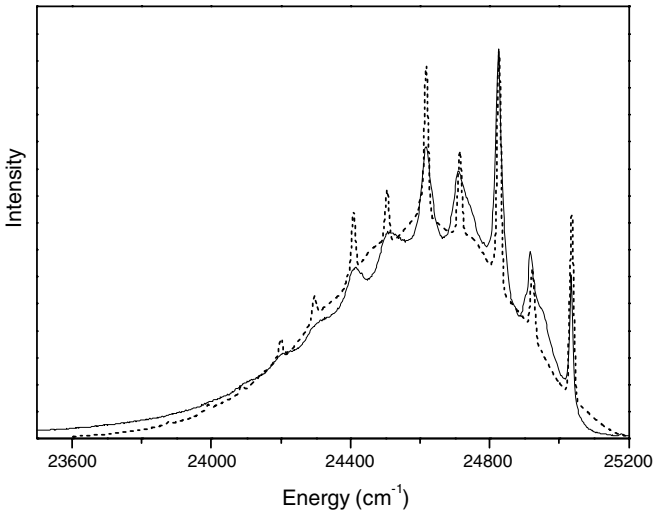

Fig. 3. Experimental (solid line) and calculated (dashed line) emission spectra for the multiphonon vibronic transitions between the lowest $(4f^6 5d)\Gamma_8$ and $(4f^7)^8S_{7/2}$ levels at the temperature of 10 K.

Table 3
Optimized parameters of the line shape function for the $(4f^6 5d)\Gamma_8 \rightarrow (4f^7)^8S_{7/2}$ transition of Eu^{2+} in $SrCl_2$

S_0	3.35
S_1	1.28
S_2	0.35
ω_0	143 cm^{-1}
ω_1	209 cm^{-1}
ω_2	113 cm^{-1}
σ_0	48 cm^{-1}
σ	4 cm^{-1}
F_{latt}	57134 cm^{-1}
F_{loc}	5033 cm^{-1}

The symbols are defined in Section 3.4.

(118 and 210 cm^{-1}), and the vibrational progressions thereupon. The spectral shape for an electronic transition coupled to two local vibrational modes can be expressed as a convolution of two spectral functions in the low temperature approximation [20]. In the present case, however, there is a broad background underlying the narrow peaks, and so a convolution of two spectral functions cannot fit the spectrum. One explanation for this broad background has been given by Wagner and Bron [21] who attributed it to lattice vibrations of a_{1g} symmetry which extend over a large frequency range, compared to those giving rise to narrow vibronic peaks. This means that the lattice modes directly induce vibronic transitions along with those induced by the local modes. Instead of subtracting the broad background from the spectrum and fitting the sharp peaks, we adopted the fitting method described in [22] where the broad background was simulated by an independent term in the line shape function. Thus an average lattice frequency ω_0 with a relatively large bandwidth σ_0 was introduced to simulate the broad background at low temperatures. The overall line shape function can be written as [22]

$$F(E) = F_{\text{latt}} \sum_{K=0}^{\infty} \frac{1}{(4\pi\sigma_0^2)^{1/2}} \frac{S_0^K \exp[-S_0]}{K!} \times \exp\left[-\frac{(E_{\text{ZPL}} - E - K\hbar\omega_0)^2}{4\sigma_0^2}\right] + F_{\text{loc}} \sum_{M=0}^{\infty}\sum_{N=0}^{\infty} \frac{1}{(4\pi\sigma^2)^{1/2}} \frac{S_1^M S_2^N \exp[-S_1 - S_2]}{M!N!} \times \exp\left[-\frac{(E_{\text{ZPL}} - E - M\hbar\omega_1 - N\hbar\omega_2)^2}{4\sigma^2}\right], \quad (2)$$

where $S_{0,1,2}$ are the Huang–Rhys factors for the average lattice and the two local vibrational modes with the frequencies $\omega_{0,1,2}$, respectively; σ_0 and σ are the widths of the individual phonon bands of Gaussian shape for the average lattice mode and the two local modes, respectively; and E_{ZPL} is the zero phonon line energy. A nonlinear least-square fitting of Eq. (2) to the experimental emission spectrum was conducted and the calculated spectrum is shown in Fig. 3. The optimized parameters are listed in Table 3.

4. Conclusions

The current interest in the spectra of Eu^{2+} resides in experimental studies of its optical applications and the theoretical aspects have been rather neglected. The present study has aimed to achieve progress in this direction and the well-resolved 10 K emission spectrum of $SrCl_2$:Eu^{2+} has been recorded and simulated. Only one $4f^6 5d$ luminescent state was observed at room temperature under various synchrotron radiation excitation energies. The low-energy 10 K absorption spectrum and the 80 K excitation spectrum are also accounted for satisfactorily by calculation.

Acknowledgements

This work is supported by the City University Research Grant 9360099. We thank the National Synchrotron Radiation Research Centre, Taiwan, for granting beam-time under Proposal 2005-3-085-3.

References

[1] J. Rubio O, J. Phys. Chem. Solids 52 (1991) 101.
[2] V.N. Vishnevsky, I.P. Pashchuk, N.S. Pidzyrailo, M.V. Tokarivsky, Ukr. Fiz. Zh. 26 (1981) 151 (in Russian).
[3] R.C. Alig, R.C. Duncan, B.J. Mokross, J. Chem. Phys. 59 (1973) 5837.
[4] J.D. Axe, P.P. Sorokin, Phys. Rev. 130 (1963) 945.
[5] T. Kobayasi, S. Mroczkowski, J.F. Owen, J. Lumin. 21 (1980) 247.
[6] S.-H. Kim et al., Jpn. J. Appl. Phys. 42 (2003) 4390.
[7] F. Pelle, T. Aitasalo, M. Lastusaari, J. Niittykoski, J. Hölsa, J. Lumin. 119 (2006) 64.
[8] X.Q. Piao, T. Horikawa, H. Hanzawa, K. Machida, Appl. Phys. Lett. 88 (2006) (Art. No. 161908).
[9] H.-C. Lu, H.-K. Chen, T.-Y. Tseng, W.-L. Kuo, M.S. Alam, B.-M. Cheng, J. Electron Spectr. Relat. Phen. C 144–147 (2005) 983.
[10] T.S. Piper, J.P. Brown, D.S. McClure, J. Chem. Phys. 46 (1967) 1353.
[11] P.A. Tanner, Top. Curr. Chem. 241 (2004) 167.
[12] D.H. Kühner, H.V. Lauer, W.E. Bron, Phys. Rev. B 5 (1972) 4112.
[13] S. Freed, S. Katcoff, Physica 14 (1948) 17.
[14] M.F. Reid, L. van Pieterson, R.T. Wegh, A. Meijerink, Phys. Rev. B 62 (2000) 14744.
[15] M.C. Downer, C.D. Cordero-Montalvo, H. Crosswhite, Phys. Rev. B 28 (1983) 4931.
[16] R.D. Cowan, The Theory of Atomic Structure and Spectra, University of California, Berkeley, 1981.
[17] H.A. Weakliem, Phys. Rev. B 6 (1972) 2743.
[18] U. Caldiño G, M.E. Villafuerte-Castrejón, J. Rubio O, Cryst. Latt. Def. Amorph. Mater. 18 (1989) 511.
[19] L. Ning, Y. Jiang, S. Xia, P.A. Tanner, J. Phys.-Condens. Matter 15 (2003) 7337.
[20] M. Wagner, J. Chem. Phys. 41 (1964) 3939.
[21] M. Wagner, W.E. Bron, Phys. Rev. B 139 (1965) A223.
[22] G.K. Liu, X.Y. Chen, J. Huang, Mol. Phys. 101 (2003) 1029.